Nanoscale

Accepted Manuscript

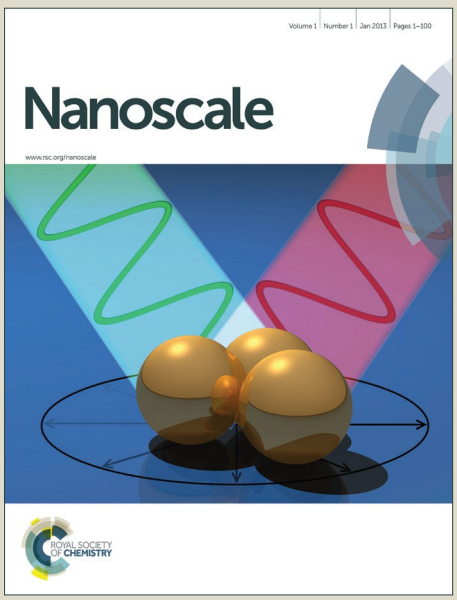

ROYAL SOCIETY OF CHEMISTRY

www.rsc.org/nanoscale

Nanoscale

COMMUNICATION

Photoluminescence Characterisations of Dynamic Aging Process of Organic-inorganic $CH_3NH_3PbBr_3$ Perovskite

Received 00th January 20xx,
Accepted 00th January 20xx

DOI: 10.1039/x0xx00000x

www.rsc.org/

R. Sheng, X. Wen,* S. Huang, X. Hao, S. Chen, Y. Jiang, X. Deng, M. A. Green and A. W. Y. Ho-Baillie

After unprecedented development of organic-inorganic lead halide perovskite solar cells over the past few years, one of the biggest barriers towards their commercialization is the stability of the perovskite material. It is thus important to understand the interaction between the perovskite material and oxygen and/or humidity and the associated degradation process in order to improve device and encapsulation design for better durability. Here we characterize the dynamic aging process in vapour-assisted deposited (VASP) $CH_3NH_3PbBr_3$ perovskite thin films using advanced optical techniques, such as time-resolved photoluminescence and fluorescence lifetime imaging microscopy (FLIM). Our investigation reveals that the perovskite grains grow spontaneously and the larger grains are formed at room temperature in the presence of moisture and oxygen. This crystallization process leads to a higher density of defects and a shorter carrier lifetime, specifically in the larger grains. Excitation-intensity-dependent steady-state photoluminescence shows both N_2 stored and aged perovskite exhibit a super-linear increase of photoluminescence intensity with increasing excitation intensity; and the larger slope in aged sample suggests a larger density of defects is generated, consistent with time-resolved PL measurements.

Introduction

Organometallic halide perovskites are attracting great research interest for next generation solar cells due to exceptional progress in device performance.[1-9] Rapidly improving power conversion efficiencies of 20.1%[3] and 10.4%[1] have been reported for methylammonium lead iodide and bromide perovskite solar cells, respectively. Moreover, organic-inorganic perovskite materials have been demonstrated as promising candidates for application in efficient light emitting diodes (LEDs) and on-chip coherent light sources due to their high photoluminescence (PL) quantum efficiencies and wavelength-tunable lasing performance.[10-12] However, the relatively poor stability of the perovskite materials is one of the largest barriers towards their commercialization.[13-15] Significant efforts have been made to understand the degradation of devices and materials, with many reports focused on device performance versus time and humidity.[16-19] Zhou et al. recently reported that by exposing the perovskite solar cell fabrication process to a low level of humidity (30%), it was possible to achieve 19.8% power conversion efficiency .[20] Another study found that using P3HT/ SWNTs-PMMA as the hole transport material (HTM) results in improved thermal stability and resistance to moisture.[21] There have also been several studies focusing on the perovskite material itself.[22, 23] In particular, enhanced crystallinity has been observed when a $CH_3NH_3PbI_{3-x}Cl_x$ film is stored under Ar,[24] and in mixed iodide-bromide perovskites reversible light-induced trap formation has been observed.[25]

Although of great importance and effort, the comprehensive physical understanding of the aging process in organic-inorganic perovskites has not yet been available. Specifically, nanoscale investigations can provide unique insights into physical phenomena occurring within the perovskite, which may be concealed by large area averaging. Fluorescence lifetime imaging microscopy (FLIM) provides nanoscale spatially- and nanosecond lifetime- resolved morphology. This technique is very suitable for perovskite solar cells, for which the solar cell performance is closely correlated with the perovskite grain morphology. In this work, we study the dynamic aging processes in $CH_3NH_3PbBr_3$ films, using steady state photoluminescence (SS-PL), time resolved PL (TRPL), FLIM and fluorescence imaging microscopy. Our results reveal that the perovskite grains keep growing spontaneously at room temperature and the larger grains are formed. We show that recrystallization during aging leads to an increased density of defects and a decreased carrier lifetime, specifically in larger grains.

Experimental section

CH_3NH_3Br was synthesized by mixing methylamine (33% in methanol, Sigma-Aldrich) with hydrobromic acid (48% in water, Sigma-Aldrich) in a 1:1 molar ratio in a 250 ml round bottom flask under continuous stirring at 0 ºC for 2 h. The

Australian Centre for Advanced Photovoltaics (ACAP)
School of Photovoltaic and Renewable Energy Engineering
University of New South Wales, Sydney 2052, Australia

Corresponding author: x.wen@unsw.edu.au

precipitate was recovered by rotary evaporation at 60 ºC, and washed three times with diethyl ether in an ultrasonic bath for 30 min. The final product was collected after dehydration at 60 ºC and dried further in a vacuum chamber overnight.

$CH_3NH_3PbBr_3$ films were deposited using the VASP method, which was originally developed by Yang Yang et. al.[47] $PbBr_2$ (1 M in DMF) was spin-coated on to a glass substrate at 2000 rpm for 60 s. After annealing at 70 ºC for 30 min, the film was treated by CH_3NH_3Br vapour for 10 min by suspending above CH_3NH_3Br powder in a closed glass petri-dish on a hotplate at 175 ºC. The treated film was then rinsed in isopropanol at room temperature. All processing was done in a N_2 glovebox.

X-ray diffraction (XRD) patterns were measured using a PANalytical Xpert Materials Research Diffractometer system with a Cu Kα radiation source (λ=0.1541 nm) at 45 kV and 40 mA. Scanning electron microscope (SEM) images were taken by an FEI Nova Nano SEM230 with TLD mode, at 3 kV and with a spot size of 2.5, SEM samples were coated with Chromium to reduce charging. Steady state PL spectra were recorded using a spectrophotometer comprising a 405 nm laser as the excitation source and a thermoelectrically cooled Si CDD detector. Fluorescence images were taken using a modified Leica TCS SP5 microscope. A 488 nm continuous-wave laser was used for excitation. The PL decay traces and fluorescence lifetime imaging spectroscopy were measured by a microtime200 microscope (Picoquant) using TCSPC technique with laser excitation at 470 nm and detection at 536 nm. The experiment was undertaken at room temperature.

Results and discussion

To monitor dynamic processes during aging of perovskite films, five $CH_3NH_3PbBr_3$/glass samples were fabricated by the VASP method in the same batch and using the same bottle of solution.[26] The films then went through different storage or aging conditions and were characterised by electron microscopy, optical microscopy, X-ray diffraction (XRD), photoluminescence measurements and fluorescence imaging.

Figure 1 shows SEM images of the six samples from the same batch. Figure 1 (a) shows the sample when it is freshly made while Figure 1 (b) shows the sample after 2 weeks of storage in N_2. Figure 1 (c); (d); (e) and (f) show the samples after 1 day; 2 days; 1 week; and 2 weeks of aging in air where the relatively humidity RH = 50%-60% and the temperature T = 25 ºC. Very little change in morphology and crystal size can be observed for the sample after 2 weeks of storage in N_2. A similar result was observed in XRD patterns which are shown in Figure 2 (a). These results reveal that N_2 suppresses any change in morphology and crystallinity.

In contrast, storage in air does have an effect on grain size. In Figure 1 (c) to (f), small grains can be seen to merge with each other to form larger grains during storage in air, and there are stretch marks on these large grains, parallel with grain boundaries. From day 7 to day 14, the stretch marks grow into contours, which have also been observed in over-annealed perovskite films.[27] A statistical analysis of the grain sizes present in these films is shown in Figure 1 (g).

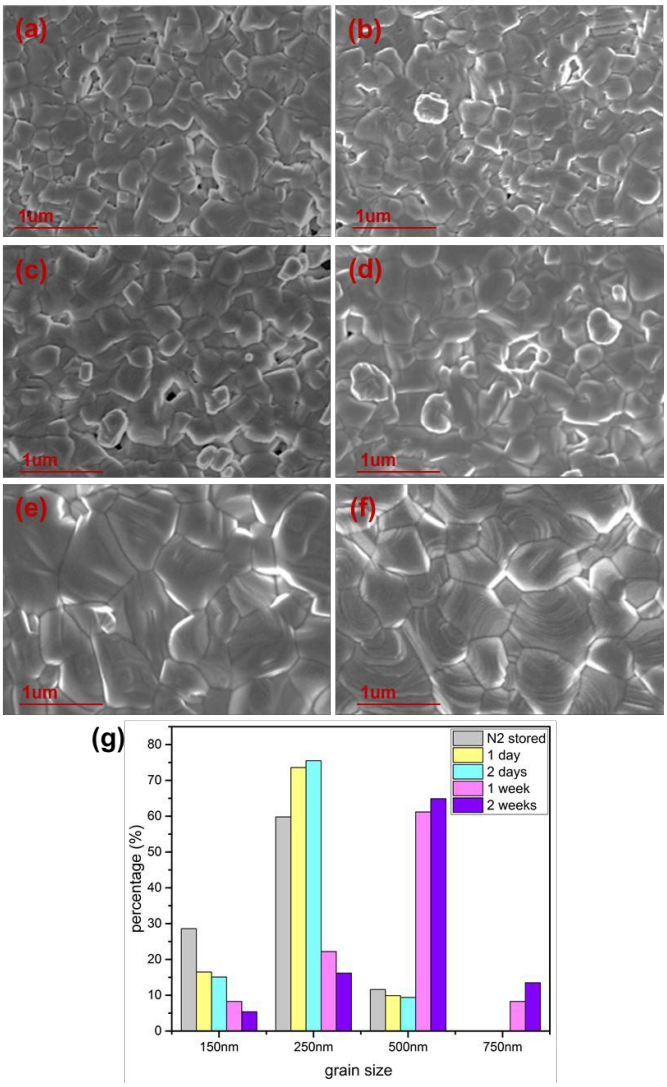

Fig 1. SEM top-view images of $CH_3NH_3PbBr_3$ films (a) when it is freshly made (b) after 2 weeks of storage in N_2, (c) after 1 day; (d) 2 days; (e) 1 week; (f) 2 weeks of aging in air where relatively humidity RH=50% to 60% and temperature T = 25 ºC. (g) Histogram of grain size at different stages.

XRD was performed on these samples to check for decomposition of $CH_3NH_3PbBr_3$ and changes in crystallinity. Figure 2 (b) shows the XRD patterns of $CH_3NH_3PbBr_3$ films before and after aging and storage in N_2 (for 2 weeks). The peaks at the 2θ values: 15.2°, 21.4°, 30.4°, 33.9°, 37.9°, 43.4°, 46.0°, correspond to the (101), (121), (040), (141), (240), (242) (060) reflections of cubic crystalline $CH_3NH_3PbBr_3$.[28] No additional peaks are detected from all aged samples. Remarkably, higher XRD counts are obtained from samples exposed to ambient air for longer periods of time. This can be attributed to enhanced crystallinity. A similar phenomenon has also been observed in mixed iodide -chloride perovskite films.[24]

To check whether the luminescence of the films changes due to aging, the steady state PL (SSPL) was measured for each sample. Figure 2(c) shows that each sample exhibits very similar SSPL, with no obvious change in peak wavelength or peak width. Furthermore, no additional PL peaks were observed between 450 and 1100 nm; for example, $PbBr_2$ has a PL peak at 2.5eV, [29] which would be present if $PbBr_2$ was generated during the aging process. In contrast, there are changes in PL lifetime and PL intensity at different stages of the aging process. This is illustrated in Figure 2 (e), where lifetime values were obtained by fitting the PL decay traces in Figure 2(d). These figures show that both the PL intensity and the effective lifetime decreases with increasing aging time, which together show that the PL quantum yield decreases with aging.

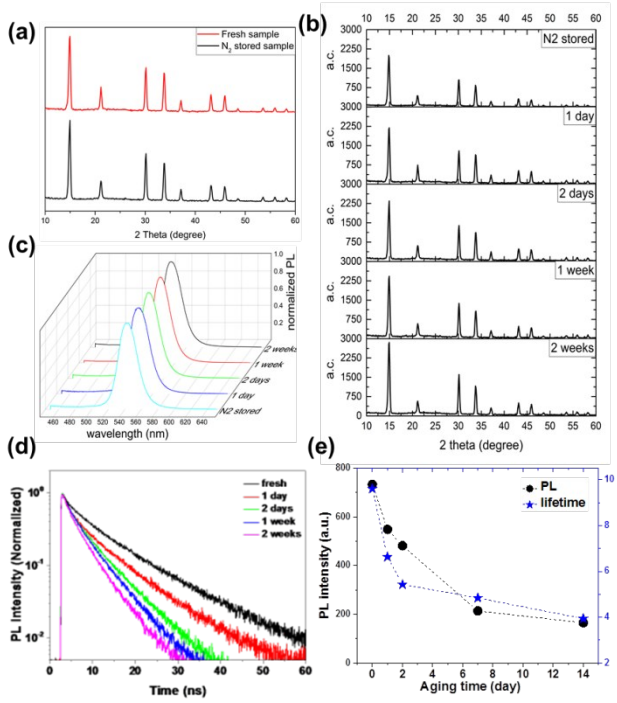

Fig 2. XRD patterns of (a) freshly made and N_2 stored (2 weeks) samples, and (b) air stored samples. (c) Steady-state PL of the $CH_3NH_3PbBr_3$ film at different aging stages. (d) PL decay traces and (e) Change in PL intensity and PL lifetime for the films over time.

To begin to understand what is occurring on the nano-scale, we measured the fluorescence images… Figure 3 (a) and (b) show the fluorescence images of N_2 stored and aged (2 weeks) $CH_3NH_3PbBr_3$ films. They agree well with the SEM images in Figure 1. The N_2-stored sample exhibits smaller grains with higher uniformity, while aged samples show the results of grain growth. It is interesting to note that there are several larger grains which exhibit lower PL intensity and so appear darker in the aged sample (Figure 3(b)). In contrast, the N_2 stored sample exhibits fairly uniform PL intensity.

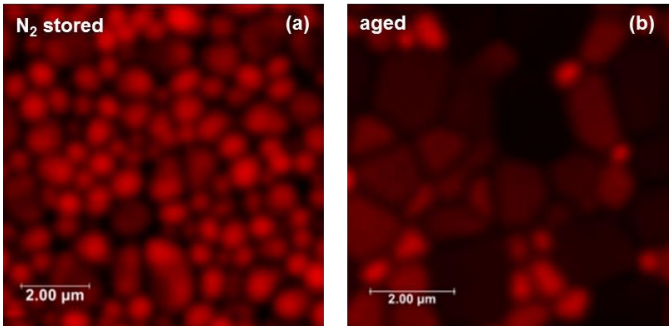

Fig 3. Fluorescence image of (a) N_2 stored (2 weeks) and (b) air stored (2 weeks) $CH_3NH_3PbBr_3$ film.

To obtain further insight into the microscopic mechanism of the aging process, we performed FLIM for the N_2 stored and aged samples based on a confocal microscope. Figure 4 (a) and (b) show the FLIM images of N_2 stored and aged (2 weeks) samples under 470 nm excitation and 536 nm detection. The N_2 stored sample exhibits small, uniformly-sized grains, with uniform and long PL lifetimes while the aged sample exhibits larger grains with lower PL intensity and shorter PL lifetimes. These observations are consistent with the SEM and optical images in Figure 1 and Figure 3, respectively. Figure 4 (c) compares the PL decay of the same N_2 stored and aged samples averaged over an area. The PL decay of the aged sample exhibits a fast component which is associated with defect trapping. [30, 31]

Figure 4 (d) compares the PL decays of a bright point (from a smaller grain) and a dark point (from a larger grain) from Figure 4(b), and the average from the observed area. Again the larger grain exhibits a fast decay component (defect trapping), and the small grain exhibits a longer lifetime and a higher PL intensity, similar to the N_2 stored sample.

The carrier dynamics in perovskite can be usually expressed as: [30, 32-34]

$$\frac{dn}{dt} = C_1 n + C_2 n^2 + C_3 n^3$$

where the terms correspond to defect trapping (Shockley-Read-Hall recombination via subgap trap states), free electron-hole recombination (bimolecular) and Auger recombination, respectively. Under low excitation intensities, defect trapping and electron-hole recombination are dominant. The observed faster decay in the darker grains implies a faster defect trapping time which in turn implies a higher defect density. [35-36]

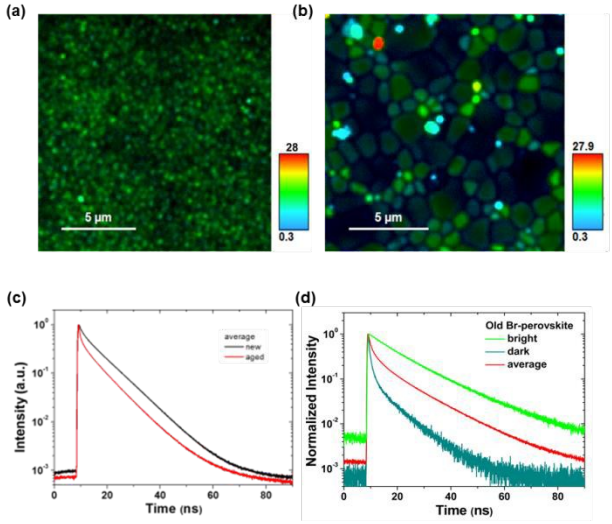

Fig 4. FLIM images of (a) N_2 stored and (b) aged (2 weeks) perovskites. The scale bar is in nanoseconds; (c) PL decay traces of the same N_2 stored and aged (2 weeks) samples averaged over a 20×20 μm^2 area, and (d) the PL decay traces from a small, bright point and a large, dark point from Figure 4 (b).

Figure 5 shows the PL intensity vs. excitation intensity in a double-logarithmic scale. Here in the low excitation regime the PL intensity exhibits a superlinear increase with increasing excitation intensity.[30] due to the correlation between the defect trapping and bimolecular recombination. The slope, *k*, of the super linearity in double-logarithmic coordinates has been shown to closely correlate with the ratio of the trap-state density to the depopulation rate of trapped states,[37] and for a general single photon excitation, where the PL intensity $I_{PL} \propto I_{EX}^{k}$,[38-42] this slope should be approximately equal to 1 if the quantum yield remains constant. For a steady state PL measurement in the low excitation range, the defect trapping and bimolecular recombination are two only possible recombination mechanisms, therefore the PL intensity is the difference of the total excitation intensity and the defect trapping. Thus, the increment of PL intensity with increasing excitation intensity can be expressed as

$$dI_{PL} = C\eta\sigma I_{Ex} \cdot (1 + f_S) \cdot dI_{Ex}$$

where I_{EX}, η, δ are excitation intensity, absorption efficiency and cross section, respectively; C is constant.[43, 44] f_s is the saturation filling factor of the defect states which is correlated with the excitation intensity, defect density and relaxation rate of the defect states. With increasing excitation intensity, the trapping by defect states will decrease due to saturation filling and slow relaxation of the defect states, which results in the super-linear increase of the electron-hole radiative recombination.

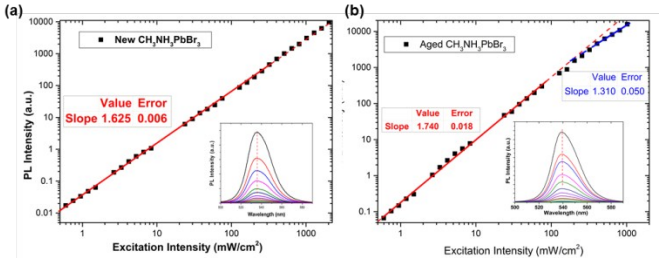

Fig 5. PL intensity as a function of excitation intensity for (a) N_2 stored and (b) aged (2 weeks) perovskite samples. Both figures are plotted on logarithmic scales so that the power factors can be obtained by linear fitting in the low excitation range.

The slope of 1.625 and 1.740 were determined for N_2 stored and aged samples, respectively. For samples of the same composition and with an identical fabrication method, it is reasonable to assume the species of the defect states and thus the relaxation rate are the same. Therefore, the saturation factor f_s is determined by the density of these defects, and the larger slope corresponds to a higher density of defects. This conclusion is consistent with the TRPL and FLIM measurements.

In Figure 4(b) the larger grains from the aged sample exhibited low PL intensity (dark) due to the presence of sub bandgap trap states.[30, 31] Numerical simulations have been done to predict defect states at several positions spanning the whole band gap of the methylamonium lead halide perovskite.[44, 45] Our study shows no spectral shape of the PL or low-energy PL band associated with defect state emission were observed, which indicate the aging generated defects are independent with the nature of the defect. This observation agrees well with other investigations of methylammonium lead iodide perovskite films.[23]

Conclusions

In summary, we have investigated the dynamic aging processes in VASP fabricated $CH_3NH_3PbBr_3$ films. The results reveal that the uniformly small grains can merge into the larger grains at room temperature in air. Such a slow process does not result in decomposition but a slow recrystallization. The larger grains were confirmed to introduce higher density of defects, exhibiting a shorter lifetime and higher super-linear slope in log-log representation of PL intensity versus excitation intensity relation. This study indicates that the $CH_3NH_3PbBr_3$ crystallises spontaneously at room temperature in air without any annealing. In nitrogen it has been shown that the crystallisation process is suppressed. Therefore, surface passivation and encapsulation is critical to maintain the quality of perovskite absorber for high performance perovskite-based devices.

Acknowledgements

Authors thank Rebecca Sutton for her kind help. The Australian Centre for Advanced Photovoltaics (ACAP) encompasses the Australian-based activities of the Australia-US Institute for Advanced Photovoltaics (AUSIAPV) and is supported by the Australian Government through the Australian Renewable Energy Agency (ARENA). This work is part of the ARENA Project 2014/RND075.

References

1. J. H. Heo, D. H. Song, S. H.Im, *Advan. Mater*., 2014: **26**, 8179.
2. N. J. Jeon, J. H. Noh, W. S. Yang, Y. C. Kim, S. Ryu, J. Seo, S. I. Seok, *Nature*, 2015. **517** (7535): p. 476-480.
3. W. S. Yang, J. H. Noh, N. J. Jeon, Y. C. Kim, S. Ryu, J. Seo, S. I. Seok, *Science*, 2015, **348** (6240), 1234-1237.
4. A. Kojima, K. Teshima, Y. Shirai, T. Miyasaka, *J. Am. Chem. Soc.*, 2009, **131** (17), 6050-6051.
5. J. H. Im, C. R. Lee, J. W. Lee, S. W. Park, N. G. Park, *Nanoscale* 2011, **3** (10), 4088-4093.
6. H. S. Kim, C. R. Lee, J. H. Im, K. B. Lee, T. Moehl, A. Marchioro, S. J. Moon, R. Humphry-Baker, J. H. Yum, J. E. Moser, M. Gratzel, N. G. Park, *Sci. Rep.* 2012, **2**, 591.
7. J. Burschka, N. Pellet, S. J. Moon, R. Humphry-Baker, P. Gao, M. K. Nazeeruddin, M. Gratzel, *Nature* 2013, **499** (7458), 316-319.
8. M. Liu, M. B. Johnston, H. J. Snaith, *Nature* 2013, **501** (7467), 395-398.
9. J. Schlipf, P. Docampo, C. J. Schaffer, V. Körstgens, L. Bießmann, F. Hanusch, N. Giesbrecht, S. Bernstorff, T. Bein, P. Müller-Buschbaum, *J. Phys. Chem. Letter*, 2015, **6** (7), 1265-1269.
10. Z. K. Tan, R. S. Moghaddam, M. L. Lai, P. Docampo, R. Higler, F. Deschler, M. Price, A. Sadhanala, L. M. Pazos, D. Credgington, F. Hanusch, T. Bein, H. J. Snaith, R. H. Friend, *Nat Nano* 2014, **9** (9), 687-692.
11. G. Xing, N. Mathews, S. S. Lim, N. Yantara, X. Liu, D. Sabba, M. Grätzel, S. Mhaisalkar, T. C. Sum, *Nat Mater* 2014, **13** (5), 476-480.
12. F. Deschler, M. Price, S. Pathak, L. E. Klintberg, D. D. Jarausch, R. Higler, S. Hüttner, T. Leijtens, S. D. Stranks, H. J. Snaith, M. Atatüre, R. T. Phillips, R. H. Friend, *J. Phys. Chem. Letter*, 2014, **5** (8), 1421-1426.
13. J. H. Noh, S. H. Im, J. H. Heo, T. N. Mandal, S. I. Seok, *Nano Letters* 2013, **13** (4), 1764-1769.
14. T. Leijtens, G. E. Eperon, S. Pathak, A. Abate, M. M. Lee, H. J. Snaith, *Nat Commun* 2013, ***4.***
15. J. A. Christians, R. C. M. Fung, P. V. Kamat, *J. Am. Chem. Soc.*, 2014, ***136*** (2), 758-764.
16. Y. Han, S. Meyer, Y. Dkhissi, K. Weber, J. M. Pringle, U. Bach, L. Spiccia, Y. B. Cheng, *J. Mater. Chem. A*, 2015, ***3*** (15), 8139-8147.
17. G. Niu, W. Li, F. Meng, L. Wang, H. Dong, Y. Qiu, *J. Mater. Chem. A*, 2014, ***2*** (3), 705-710
18. C. Law, L. Miseikis, S. Dimitrov, P. Shakya-Tuladhar, X. Li, P. R. Barnes, J. Durrant, B. C. O'Regan, *Adv. Mater*. 2014, ***26*** (36), 6268-6273
19. Y. Yamada, M. Endo, A. Wakamiya, Y. Kanemitsu, *J. Phys. Chem. Letter* 2015, ***6*** (3), 482-486.
20. H. Zhou, Q. Chen, G. Li, S. Luo, T. B. Song, H. S. Duan, Z. Hong, J. You, Y. Liu, Y. Yang, *Science* 2014, ***345*** (6196), 542-546.
21. S. N. Habisreutinger, T. Leijtens, G. E. Eperon, S. D. Stranks, R. J. Nicholas, H. J. Snaith, *Nano Letters* 2014, ***14*** (10), 5561-5568.
22. J. A. Christians, P. A. Miranda Herrera, P. V. Kamat, *J. Am. Chem. Soc.*, 2015, ***137*** (4), 1530-1538.
23. J. F. Galisteo-López, M. Anaya, M. E. Calvo, H. Míguez, *J. Phys. Chem. Letter*, 2015, ***6*** (12), 2200-2205.
24. B. W. Park, B. Philippe, T. Gustafsson, K. Sveinbjörnsson, A. Hagfeldt, E. M. J. Johansson, G. Boschloo, *Chem. Mater.*, 2014, ***26*** (15), 4466-4471.
25. E. T. Hoke, D. J. Slotcavage, E. R. Dohner, A. R. Bowring, H. I. Karunadasa, M. D. McGehee, *Chem. Sci.* 2015, ***6*** (1), 613-617.
26. R. Sheng, A. Ho-Baillie, S. Huang, S. Chen, X. Wen, X. Hao, M. A. Green, *J. Phys. Chem. C*, 2015, ***119*** (7), 3545-3549.
27. G. E. Eperon, V. M. Burlakov, P. Docampo, A. Goriely, H, J, Snaith, *Adv. Funct. Mater.* 2014, ***24*** (1), 151-157.
28. E. Edri, S. Kirmayer, D. Cahen, G. Hodes, *J. Phys. Chem. Letter*, 2013, ***4*** (6), 897-902.
29. M. Iwanaga, M. Watanabe, T. Hayashi, *Phy. Rev. B*, 2000, ***62*** (16), 10766-10773.
30. M. Saba, M. Cadelano, D. Marongiu, F. Chen, V. Sarritzu, N. Sestu, C. Figus, M. Aresti, R. Piras, A. G. Lehmann, *Nat. Com.* 2014, ***5,*** 5049.
31. S. D. Stranks, V. M. Burlakov, T. Leijtens, J. M. Ball, A. Goriely, H. J. Snaith, *Phy. Rev. Appl.* 2014, ***2*** (3), 034007.
32. J. S. Manser, P. V. Kamat, *Nat. Photon.* 2014, ***8*** (9), 737-743.
33. C. Wehrenfennig, M. Liu, H. J. Snaith, M. B. Johnston, L. M. Herz, *Eng. Environ. Sci.* 2014, ***7*** (7), 2269-2275.
34. C. S. Ponseca, R. J. Savenije, M. Abdellah, K. Zheng, A. Yartsev, T. Pascher, T. Harlang, P. Chabera, T. Pullerits, A. Stepanov, J. P. Wolf, V. Sundstrom, *J. Am. Chem. Soc.* 2014, ***136*** (14), 5189-5192.
35. Y. Yamada, T. Nakamura, M. Endo, A. Wakamiya, Y. Kanemitsu, *J. Am. Chem. Soc.* 2014, ***136*** (33), 11610-11613.
36. X. Wang, Z. Feng, J. Shi, G. Jia, S. Shen, J. Zhou, C. Li, *Phys. Chem. Chem. Phys.* 2010, ***12*** (26), 7083-7090.
37. X. Wen, Y. Feng, S. Huang, F. Huang; Y Cheng, M. Green, A. Ho-Baillie, *J. Mater. Chem. C*, to be published.
38. X. Wen, P. Yu, Y. R. Toh, X. Ma, J. Tang, *Chem. Comm.* 2014, ***50*** (36), 4703-4706.
39. X. Wen, R. Sheng, A. W. Ho-Baillie, A. Benda, S. Woo, Q. Ma, S. Huang, M. A. Green, *J. Phys. Chem. Lett.* 2014, ***5*** (21), 3849-3853.
40. J. R. Lakowicz, *Springer Science & Business Media*: 2013.
41. W. Denk, J. H. Strickler, W. W. Webb, *Science* 1990, ***248*** (4951), 73-76.
42. B. R. Masters, P. So, E. Gratton, *Biophys. J.* 1997, ***72*** (6), 2405.
43. X. Wen, P. Zhang, T. A. Smith, R. J. Anthony, U. R. Kortshagen, P. Yu, Y. Feng, S. Shrestha, G. Coniber, S. Huang, *Sci. Rep.* 2015, ***5,*** 12469.
44. X. Wen, L. Dao, P. Hannaford, S. Mokkapati, H. Tan, C. Jagadish, *J. Phys.: Condens. Matter*, 2007, ***19*** (38), 386213.

45. W. J. Yin, T. Shi, Y. Yan, *Appl. Phy. Lett.*, 2014, ***104*** (6), 063903.
46. A. Buin, P. Pietsch, J. Xu, O. Voznyy, A. H. Ip, R. Comin, E. H. Sargent, *Nano Lett.*, 2014, ***14*** (11), 6281-6286.
47. Chen, Q.; Zhou, H.; Hong, Z.; Luo, S.; Duan, H.-S.; Wang, H.-H.; Liu, Y.; Li, G.; Yang, Y., *J. Am. Chem. Soc.*, 2013, ***136*** (2), 622-625.